PAPER

Understanding of multiple resistance states by current sweeping in MoS_2-based non-volatile memory devices

IOP Publishing Nanotechnology

Nanotechnology **31** (2020) 465206 (7pp) https://doi.org/10.1088/1361-6528/aba46a

Understanding of multiple resistance states by current sweeping in MoS_2-based non-volatile memory devices

Xiaohan Wu, Ruijing Ge, Deji Akinwande and Jack C Lee

Microelectronics Research Center, Department of Electrical and Computer Engineering, The University of Texas at Austin, Austin, Texas 78758, United States of America

E-mail: leejc@austin.utexas.edu and deji@ece.utexas.edu

Received 10 May 2020, revised 8 June 2020
Accepted for publication 9 July 2020
Published 26 August 2020

Abstract

Recently, various two-dimensional materials have been reported to exhibit non-volatile resistance switching phenomenon. The atomristors, featuring memristor effect in atomically thin nanomaterials such as monolayer transition metal dichalcogenides and hexagonal boron nitride, have drawn much attention due to the extremely thin active layer thickness with the advantages of forming-free characteristic, large on/off resistance ratio and fast switching speed. To investigate the switching mechanisms in the 2D monolayers, we introduced an electrical characterization method by current sweeping to illustrate the detailed information hidden in the commonly used voltage-sweep curves. Multiple transition steps have been observed in the SET process of MoS_2-based resistance switching devices. The different behaviors of transition steps were attributed to the number of defects or vacancies associated with the switching phenomenon, which is consistent with the previously reported conductive-bridge-like model for 2D atomristors. This work provides an approach using current sweeping to precisely characterize the resistance switching effect and inspires further research to optimize the defect distribution in 2D materials for the applications in multi-bit non-volatile memory and neuromorphic computing.

Supplementary material for this article is available online

Keywords: 2D materials, non-volatile memory, resistance switching, current sweeping

(Some figures may appear in colour only in the online journal)

1. Introduction

Two-dimensional (2D) materials are crystalline nanomaterials consisting of a single or few layers of atoms. Since the report of graphene as the first 2D material in 2004, many other 2D materials have been identified and studied, including transition metal dichalcogenides (TMDs), hexagonal boron nitride (h-BN), black phosphorus, silicene, etc [1–6]. Benefiting from the diverse mechanical, chemical, optical and electrical properties of various 2D materials, a wide range of applications have been developed for the next-generation electron devices, optoelectronics, flexible electronics and biosensors [7–10]. One of the applications is the non-volatile resistance switching (NVRS) devices, also referred to as resistive random access memory (RRAM), as an emerging non-volatile memory with the advantages of high density, low power consumption, fast switching speed and good reliability [11–14]. The resistance of the NVRS devices can be

repeatably switched between a high resistance state (HRS) and a low resistance state (LRS) through external electrical bias and subsequently sustained without any power. A typical structure of NVRS devices, known as metal-insulator-metal (MIM), consists of an active layer that exhibits resistance switching property sandwiched between two metallic electrodes. The traditional active layer materials are bulk metal oxide films, while in the last few years, the NVRS behavior has been observed in various 2D materials as well, including functionalized graphene oxide, degraded black phosphorus and single- or multi-layer h-BN [15–18]. As a representative TMD material, molybdenum disulfide (MoS_2) has drawn much attention due to its direct bandgap in monolayers and the application in 2D-based flexible field-effect transistors [8]. In addition, MoS_2 has been reported to be used as the active NVRS layer in the form of 1 T-phase MoS_2 nanosheet, grain boundary assisted planar MoS_2 monolayer, and vertical MoS_2 double layers [19–21]. In 2018, it was reported that monolayer MoS_2, as well as other TMDs ($MoSe_2$, WS_2 and WSe_2), exhibits intrinsic NVRS behavior in vertical MIM configuration, which demonstrates that resistance switching is accessible in atomically thin 2D monolayers [22, 23]. These devices, collectively labeled as atomristors, show stable switching with forming-free characteristic, high on/off current ratio, fast switching speed, and demonstrated applications in flexible memory devices and RF switches. Compared with state-of-the-art metal-oxide RRAM devices, the atomristors, at a nascent state, have the limitation of relatively low yield and endurance. However, the performance is expected to be improved with optimized fabrication processes and advanced device structures.

Voltage-sweep electrical measurement is a characterization method commonly used to obtain basic I–V curves and extract resistance switching parameters, such as switching voltages, LRS or HRS resistance and on/off current ratio [11]. However, due to the voltage-triggered mechanism of SET process (switching from HRS to LRS), the voltage-sweep method can only reveal the critical SET voltage, and not much more. Current-sweep measurement has been used in the bulk metal-oxide RRAM devices and shows diverse switching behavior [24–26]. Nevertheless, this method has not been applied to the 2D-based NVRS devices. Herein, in addition to voltage-sweep measurement, we performed electrical measurement by current sweeping to get more insights into the intriguing SET characteristics and enhance the understanding of the switching mechanisms of atomristors. The results show that, in contrast to the one-step sharp transition in most of the voltage-sweep curves, the resistance can have multiple resistance reduction steps during the SET process as illustrated by current sweeping. Moreover, various resistance transition steps can be observed in different devices or in different cycles of the same device. This phenomenon can be explained by the effect of multiple conductive links originated from localized defects in the 2D atomic layers, consistent with reported *ab-initio* simulation results [18]. Multiple resistance states can be easily obtained and clearly identified through the current-sweep method. This is beneficial to the fundamental understanding of 2D-based memory devices and inspires applications in multi-bit data storage and analog-like neuromorphic computing.

2. Device fabrication and characterization

Continuous single-layer or 3–5 layers MoS_2 films purchased from SixCarbon Technology were synthesized on SiO_2/Si substrate by chemical vapor deposition (CVD). Crossbar atomristor devices were prepared on another SiO_2/Si substrate or a commercial diamond substrate. Bottom electrodes (BE) were patterned by electron beam lithography and deposited with a 2 nm Cr/100 nm Au metal stack using electron beam evaporation. The MoS_2 film was then transferred onto the target substrate by a polydimethylsiloxane (PDMS) stamp transfer method. In this method, the MoS_2 film was brought into conformal contact with PDMS stamp. The substrate-MoS_2-PDMS system was then soaked into diluted water. The SiO_2 on the substrate is hydrophilic, which makes it easy for water to diffuse into the interface between MoS_2 and SiO_2. The MoS_2-PDMS film was separated from SiO_2/Si substrate and brought into contact with the target substrate with BE on it. Subsequently, the PDMS stamp was peeled off, leaving MoS_2 on the target substrate. After transferring, top electrodes (TE) were patterned and deposited using the same fabrication method as BE. The devices were measured on a Cascade probe station with an Agilent 4156 semiconductor parameter analyzer under ambient conditions for both voltage and current sweeping measurements. Raman spectroscopy and photoluminescence (PL) were performed to evaluate the MoS_2 film before transferring on a Renishaw in-Via system using a 532 nm wavelength source.

3. Results and discussion

The schematic of fabricated crossbar MoS_2 atomristors is illustrated in figure 1(a) with the vertical MIM device structure, which consists of the MoS_2 film sandwiched between two metallic electrodes. To eliminate the possible effect of metal oxide from electrodes, the inert metal—gold, was used as the electrode material of the devices. The device area is defined as the overlapped region between the top and bottom electrodes. Optical microscope image is presented in figure 1(b) to evaluate a representative MoS_2 NVRS device on SiO_2/Si substrate with CVD-grown MoS_2 film after transferring. To further characterize the MoS_2 films, Raman spectroscopy and PL were performed, demonstrating the high quality of the layered crystalline 2D material as displayed in figure 1(c) [27, 28]. The PL peak position for monolayer MoS_2 is located at 1.85 eV, in good agreement with the reported optical band gap.

Figure 1(d) shows a representative voltage-sweep bipolar I–V curve of a crossbar MoS_2 NVRS device. Initially, the as-fabricated device is at a high-resistance state (HRS). A positive voltage bias is applied to the device by voltage sweeping, leading to a sharp increase of current at ~2.9 V. The resistance state is switched from a HRS to a low resistance state

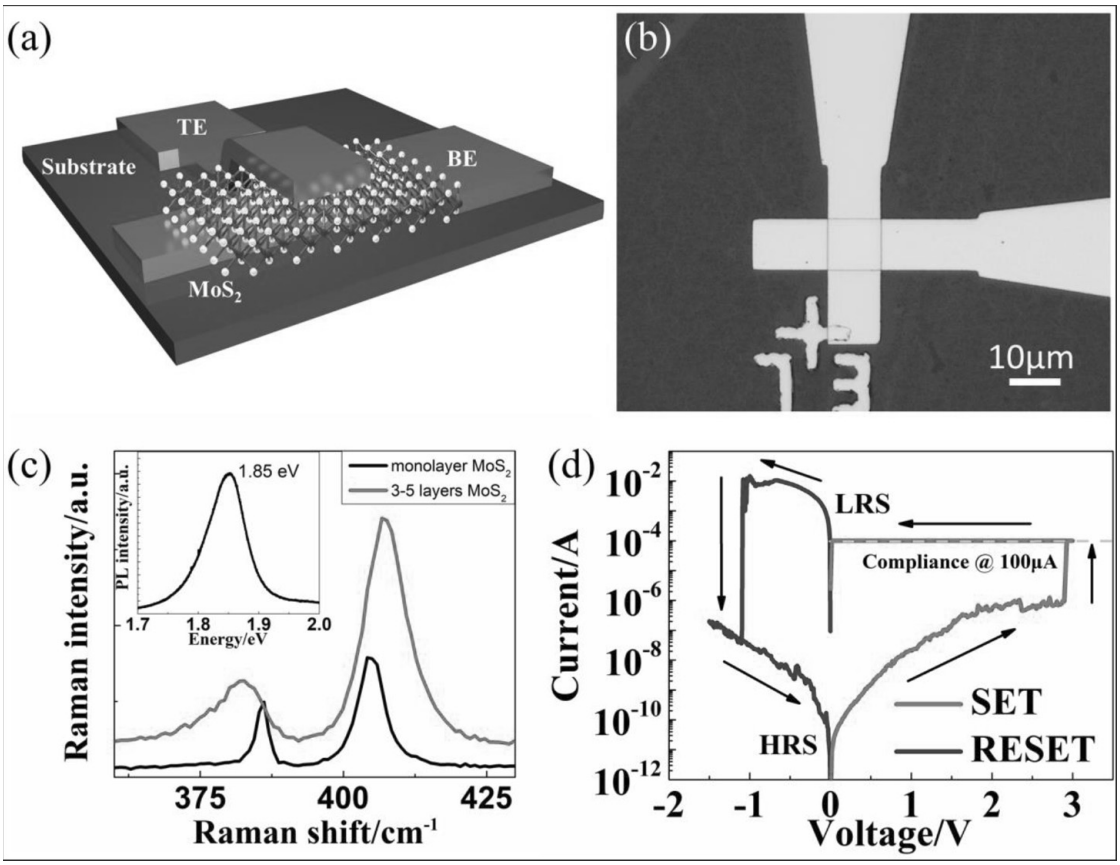

Figure 1. (a) The schematic of the crossbar atomristor with monolayer MoS_2 as the active layer. (b) The optical image of fabricated monolayer MoS_2 crossbar device with Au electrodes on SiO_2/Si substrate. The device area (10 x 10 μm^2 for this device) is defined by the overlapped region between TE and BE. (c) Raman and PL spectrum of CVD-grown monolayer and 3–5 layers MoS_2 films. The inset shows the PL peak position of monolayer MoS_2 at 1.85 eV. The spectra are consistent at different locations of the sample, indicating a uniform MoS_2 film. (d) A representative voltage-sweep I–V curve in MoS_2 crossbar device on diamond substrate with lateral area of 0.5 $\times$ 0.5 μm^2. A compliance current during SET is usually needed to protect the device. One sharp current increasing step is observed in the SET process.

(LRS), which is commonly referred to as a 'SET' process. A compliance current (100 μA in this case) is applied to the device to prevent irreversible breakdown during the SET process due to unconstrained high current. The device will remain at LRS without external power supply, until a voltage bias at ~ − 1.1 V is applied on the device by a negative voltage sweeping to 'RESET' it back to HRS. Unlike most traditional metal oxide NVRS materials, the 2D layered materials based NVRS devices require no electro-forming process, which initializes a soft dielectric breakdown for conductive filament formation before resistance switching cycling in bulk metal oxides [11]. In addition to the relatively low switching voltages (down to < 1 V as reported in our previous works), a high on/off current ratio can be obtained based on the MoS_2 atomristors (~ 10^6 from this I–V curve) [22]. Note that using voltage sweeping method, typical transition from HRS to LRS is a sharp current increase. The straightforward inference from this phenomenon is that the SET process could be a single-step physics transition directly from a HRS to a LRS. However, based on the previous study, multiple resistance states can be obtained by changing the compliance current during SET process [22]. This contradiction suggests that detailed information is likely to be hidden behind the voltage-sweep I–V characteristics.

To further study the resistance switching phenomenon during SET process in the MoS_2 atomristors, the current-sweep measurements were performed to the devices to achieve a more comprehensive understanding. Figure 2(a) displays the voltage-current relationship by current sweeping method to SET a MoS_2 NVRS device on SiO_2/Si substrate. The transition starts at a HRS, followed by a gradual increase of both voltage and current. As the current reaches ~1.8 mA, the voltage suddenly drops while the conduction current remained the same. In other words, the resistance of the device is switched from a higher resistance state to a lower resistance state. Four subsequent voltage decreasing steps can be observed from 0.01 A to 0.03 A (shown in the amplified figure as the inset). The device remains at the final lowest resistance state during and after the backward sweeping, which indicates a non-volatile resistance switching process from HRS to LRS (SET) is realized by current sweep. Figure S1(https://stacks.iop.org/NANO/31/465206/mmedia) shows

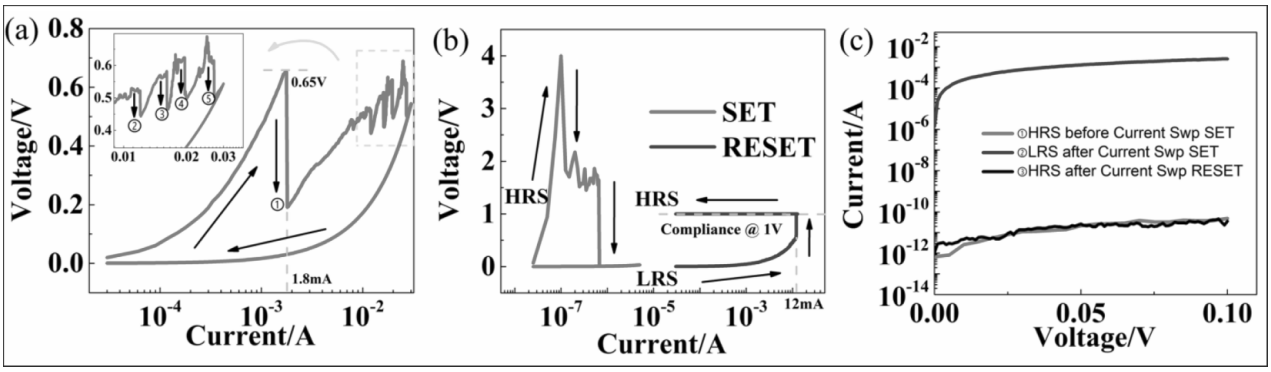

Figure 2. (a) A representative resistance switching curve of current-sweep SET process. Five separate resistance reduction steps can be seen in this figure. The tested device is a monolayer MoS_2 device on SiO_2/Si substrate with lateral area of $10 \times 10\ \mu m^2$. (b) The complete switching curve consisting of SET and RESET process by current sweeping. A compliance voltage during RESET is needed to protect the device. The tested device is a 3–5 layers MoS_2 device on diamond substrate with lateral area of $0.3 \times 0.3\ \mu m^2$. (c) The 'READ' curves before and after current sweeping SET and RESET. A large on/off ratio of ~10^7 can be obtained.

the same current-sweep SET process as figure 2(a) in the form of resistance-current curve. Voltage-sweep method is applied on the same device as figure 2(a) and the switching I–V curve is shown in figure S2. Compared with the single-step SET by voltage sweep, multiple transition steps can be observed during current-sweep measurement. It is also worth noting that the voltage for the first transition in current sweeping is ~0.65 V, which is very close to the SET voltage using voltage sweeping on the same device.

In order to achieve better performance on small-area devices, diamond substrates are used in the fabrication of the MoS_2 atomristors. Compared with SiO_2/Si substrate, which has a relatively low thermal conductivity for SiO_2 ($1.4\ W \cdot m^{-1} \cdot K^{-1}$), the diamond substrate with a high thermal conductivity at ~$1000\ W \cdot m^{-1} \cdot K^{-1}$ can dissipate the excessive heat through the substrate more effectively, preventing the narrow metal lines of the electrodes from Joule heating and thus enabling the fabrication of small-area crossbar devices. According to the area-dependence study of MoS_2 atomristors, the HRS resistance scales inversely with area due to uniform conduction, while LRS resistance, determined by the conductive link(s), is invariant with area, leading to a larger on/off ratio for small-area devices [22]. Moreover, the switching voltages tend to be relatively large for devices with smaller area because of less localized defects associated with the resistance switching behavior. The results in figure 2(b) are consistent with the area-dependence characteristics, showing larger on/off ratio and higher triggering voltage (the first transition for SET happens at ~4 V). The lateral device area in figure 2(b) is $0.3 \times 0.3\ \mu m^2$, which is about ~1000x smaller than the one shown in figure 2(a) on Si/SiO_2 substrate. Similarly, a multiple-step SET can be observed by current sweep. In addition, the RESET process realized by current-sweep measurement is presented in the same figure. As the current sweeps to ~12 mA, the voltage abruptly increases, indicating a transition from LRS to HRS. This transition current is consistent with the RESET current (~10 mA) by voltage sweep method. Compared with RESET behavior using voltage sweep, a compliance voltage is required to avoid extremely high voltage across the device. Voltage-sweep method is applied on the same device as figure 2(b) and the switching I–V curve is shown in figure S3. From the comparison of the two operation methods, the current-sweep RESET only has one transition step, while voltage-sweep RESET has multiple steps. It can thus be inferred that the RESET process is more likely to be a current/thermal-driven effect instead of voltage-driven effect. During RESET, the Joule heating induced by the high RESET current will dissolve the conductive path first and then the Au ions will be migrated though porous regions or defects in the MoS_2 film, or back to the electrodes by reduction [11, 29, 30]. The effect of Joule heating is supported by the experimental observation that the transitions in voltage-sweep RESET of the MoS_2 memory devices, although sometimes with multiple steps, are sharp and sudden instead of gradual changes, which is a signature of Joule heating-dominated RESET process. Another evidence is that the MoS_2-based NVRS device can be switched by both bipolar and unipolar operation, which means it is not the electrical bias but the current level that plays a more essential role in the RESET switching. The 'READ' operations were performed on the device before and after the current-sweep switching as shown in figure 2(c), which demonstrates the non-volatility nature of the resistance switching behavior with a large on/off ratio of ~10^7. The resistance state after current-sweep RESET is consistent with the initial HRS state, indicating the stable switching characteristics and alluding to a potential approach using current sweeping to improve the cycle-to-cycle variability at HRS, a long-standing issue for RRAM devices [31].

Figures 3(a) and (c) present the switching curves of the SET by current sweeping and RESET by voltage sweeping respectively on the same device. Similarly, the switching characteristics for current-sweep SET and voltage-sweep RESET obtained on another device are shown in figures 3(b) and (d). Based on the collected data of all the tested devices, a correlation can be established: normally for a device with

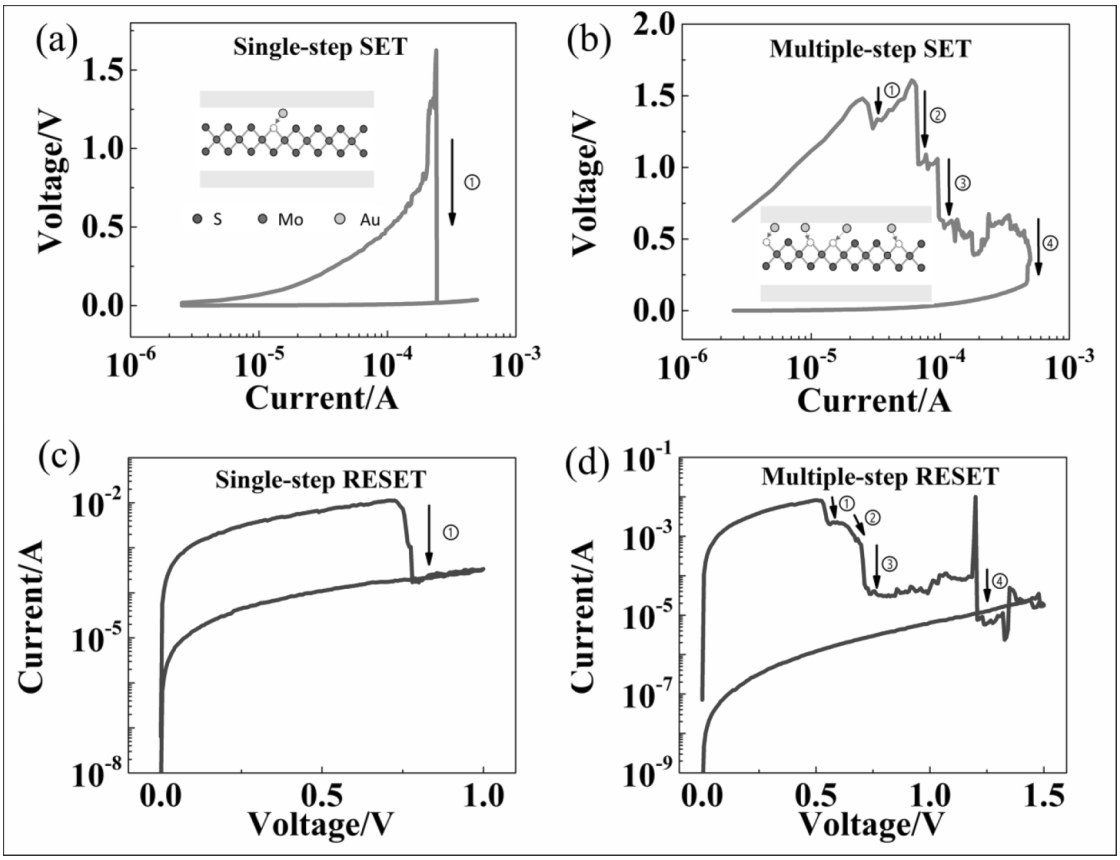

Figure 3. The resistance switching characteristics of (a) current-sweep SET and (c) voltage-sweep RESET on the same device with similar single-step transition behavior. The resistance switching characteristics of (b) current-sweep SET and (d) voltage-sweep RESET on the same device with similar multiple-step transition behavior. The variation in transition steps can be attributed to the different number of sulfur vacancies that attract gold ions to form single or multiple conductive links (illustrated in the insets).

single-step SET behavior by current sweeping (figure 3(a)), the voltage-sweep RESET is also single-step (figure 3(c)), while for a device that has multiple steps during current-sweep SET (figure 3(b)), a multiple-step RESET can be observed by voltage sweeping (figure 3(d)). The statistical results (see table S1) show that among all the 16 tested devices, 12 of them follow the correlation that the transition step number matches between current-sweep SET and voltage-sweep RESET. For the other four devices, the difference between the transition step number is only 1, which could be attributed to the cycle-to-cycle variation. In our previous studies of switching mechanisms based on *ab-initio* simulation, we proposed a conductive-bridge-like model with assistance of the metal ion migration. The current-sweep switching characteristics provide additional evidence for this model and can be explained by the single or multiple metal ions substitution into the localized sulfur vacancies. During the SET process, the metal atoms at the positive biased electrodes lose electrons and become positively charged ions. The metal ions are then attracted by the sulfur vacancies in the MoS_2 film and reduced subsequently, forming a conductive path through the substituting metal, which indicates the transition from HRS to LRS. An atomic-level model is proposed here to explain the switching behavior: First, a metal atom (ion) dissociates from a cluster of metal atoms in the electrodes. The dissociation step is dominated by the atomization enthalpy of the metal (Au has relatively low atomization enthalpy). Second, the metal atom (ion) diffuses across 2D material surface until it migrates to a favorable location for the following reaction. Finally, the metal atom (ion) is absorbed into defects in 2D materials (most commonly sulfur vacancies in MoS_2 film). With the experimental results in this work that show multiple transition steps, it can be inferred that multiple defect/vacancy-rich regions exist within the device area, which leads to multiple conductive links formation during switching. Au is not commonly used as the electrodes in bulk material-based conductive-bridge RAM due to relatively high work function. However, for the atomically thin 2D materials, a small portion of Au ions from electrodes is enough to form the conductive path in a localized area and produces resistance switching. In addition, the migration of Au in MoS_2 film has been demonstrated experimentally and theoretically with a low migration energy barrier of ~0.1 eV, which supports the proposed mechanisms based on Au migration as mentioned above [32, 33]. Depending on the number of defects or vacancies associated with the switching, single-step (figure 3(a)) or multiple-step (figure 3(b))

transition can be obtained in different devices. Limited by relatively low yield and large variability of 2D-based NVRS devices at an early stage, the dependence of device area and thickness on current-sweep behavior cannot be directly observed. However, it is expected to be illustrated in the future with the optimization on material growth, device fabrication and testing technology. The various resistance states were not directly observed in voltage-sweep measurement since the SET process is dominated by the external electric field. Once the voltage increases beyond the critical value, the device will be suddenly switched, resulting in one sharp transition in the I–V curve. Using the current-sweep measurement, the hidden details of the various resistance states and the associated defect information can be illustrated. Besides the RESET process, it is now shown that in SET process, multiple transition steps can be realized and directly monitored in the switching curves. Analog-like synaptic devices based on multiple resistance states transition can benefit from the current-sweep method with more information revealed, which inspires potential operation by current signal as input to trigger the gradual resistance switching effect. With the precise manipulation of resistance and more comprehensive study of underlying physics, it is expected that the MoS_2-based NVRS device will be a promising candidate in neuromorphic applications.

4. Conclusion

In conclusion, we elucidate the non-volatile resistance switching behavior in MoS_2-based atomristors using current-sweep measurement method, which shows multiple resistance transition steps in SET process compared with one sharp transition by voltage-sweep measurement. A correspondence between current-sweep SET and voltage-sweep RESET with the same characteristics of transition steps can be observed, alluding to the effect of defects or vacancies in the 2D atomic sheets associated with the resistance switching phenomenon. These results provide additional experimental support for the single or multiple conductive links model with the assistance of metal ions migration. This paper suggests a promising approach to characterize the NVRS phenomenon in not only 2D atomristors but also other resistive switching devices, inspires further theoretical or experimental studies of the switching mechanisms in the atomically thin monolayer materials, and paves the way for defect engineering to meet diverse requirements in various applications including multi-bit data storage, low-power RF switch and neuromorphic computing.

Acknowledgments

This work was supported in part by the National Science Foundation (NSF) grant #1809017. The authors acknowledge use of Texas Nanofabrication Facilities supported by the NSF NNCI award #1542159. D.A. acknowledges the Presidential Early Career Award for Scientists and Engineers (PECASE) through the Army Research Office (W911NF-16-1-0277). The authors appreciate Jo Wozniak of Texas Advanced Computing Centre (TACC) for 3D renderings.

ORCID iD

Xiaohan Wu https://orcid.org/0000-0002-0050-7616

References

[1] Akinwande D, Huyghebaert C, Wang C H, Serna M I, Goossens S, Li L J, Wong H P and Koppens F H L 2019 Graphene and two-dimensional materials for silicon technology *Nature* **573** 507–18

[2] Novoselov K S, Geim A K, Morozov S V, Jiang D, Zhang Y, Dubonos S V, Grigorieva I V and Firsov A A 2004 Electric field effect in atomically thin carbon films *Science* **306** 666–9

[3] Radisavljevic B, Radenovic A, Brivio J, Giacometti V and Kis A 2011 Single-layer MoS2 transistors *Nat. Nanotechnol.* **6** 147–50

[4] Tao L, Cinquanta E, Chiappe D, Grazianetti C, Fanciulli M, Dubey M, Molle A and Akinwande D 2015 Silicene field-effect transistors operating at room temperature *Nat. Nanotechnol.* **10** 227–31

[5] Park J H *et al* 2014 Large-area monolayer hexagonal boron nitride on Pt foil *ACS Nano* **8** 8520–8

[6] Ling X, Wang H, Huang S, Xia F and Dresselhaus M S 2015 The renaissance of black phosphorus *Proc. Natl Acad. Sci. USA* **112** 4523–30

[7] Wang Q H, Kalantar-Zadeh K, Kis A, Coleman J N and Strano M S 2012 Electronics and optoelectronics of two-dimensional transition metal dichalcogenides *Nat. Nanotechnol.* **7** 699–712

[8] Akinwande D, Petrone N and Hone J 2014 Two-dimensional flexible nanoelectronics *Nat. Commun.* **5** 5678

[9] Molle A, Goldberger J, Houssa M, Xu Y, Zhang S C and Akinwande D 2017 Buckled two-dimensional Xene sheets *Nat. Mater.* **16** 163–9

[10] Lee J, Dak P, Lee Y, Park H, Choi W, Alam M A and Kim S 2014 Two-dimensional layered MoS(2) biosensors enable highly sensitive detection of biomolecules *Sci. Rep.* **4** 7352

[11] Wong H S P, Lee H, Yu S, Chen Y, Wu Y, Chen P, Lee B, Chen F T and Tsai M 2012 Metal-oxide RRAM *Proc. IEEE* **100** 20

[12] Z F, C. Y-F, B K, F B and L J C 2014 Characterization of external resistance effect and performance optimization in unipolar-type SiOx-based resistive switching memory *Appl. Phys. Lett.* **105** 133501

[13] Chen Y C, Hu S T, Lin C Y, Fowler B, Huang H C, Lin C C, Kim S, Chang Y F and Lee J C 2018 Graphite-based selectorless RRAM: improvable intrinsic nonlinearity for array applications *Nanoscale* **10** 15608–14

[14] Chen Y C, Lin C C, Hu S T, Lin C Y, Fowler B and Lee J 2019 A novel resistive switching identification method through relaxation characteristics for sneak-path-constrained selectorless RRAM application *Sci. Rep.* **9** 12420

[15] Hao C *et al* 2016 Liquid-exfoliated black phosphorous nanosheet thin films for flexible resistive random access memory applications *Adv. Funct. Mater.* **26** 2016–24

[16] Pan C *et al* 2017 Coexistence of grain-boundaries-assisted bipolar and threshold resistive switching in multilayer hexagonal boron nitride *Adv. Funct. Mater.* **27** 1604811

[17] Pradhan S K, Xiao B, Mishra S, Killam A and Pradhan A K 2016 Resistive switching behavior of reduced graphene oxide memory cells for low power nonvolatile device application *Sci. Rep.* **6** 26763

[18] Wu X, Ge R, Chen P A, Chou H, Zhang Z, Zhang Y, Banerjee S, Chiang M H, Lee J C and Akinwande D 2019 Thinnest nonvolatile memory based on monolayer h-BN *Adv. Mater.* **31** e1806790
[19] Cheng P, Sun K and Hu Y H 2016 Memristive behavior and ideal memristor of 1T phase MoS2 *Nanosheets Nano Lett.* **16** 572–6
[20] Sangwan V K, Jariwala D, Kim I S, Chen K S, Marks T J, Lauhon L J and Hersam M C 2015 Gate-tunable memristive phenomena mediated by grain boundaries in single-layer MoS2 *Nat. Nanotechnol.* **10** 403–6
[21] Xu R, Jang H, Lee M H, Amanov D, Cho Y, Kim H, Park S, Shin H J and Ham D 2019 Vertical MoS2 double-layer memristor with electrochemical metallization as an atomic-scale synapse with switching thresholds approaching 100 mV *Nano Lett.* **19** 2411–7
[22] Ge R, Wu X, Kim M, Shi J, Sonde S, Tao L, Zhang Y, Lee J C and Akinwande D 2018 Atomristor: nonvolatile resistance switching in atomic sheets of transition metal dichalcogenides *Nano Lett.* **18** 434–41
[23] Kim M, Ge R, Wu X, Lan X, Tice J, Lee J C and Akinwande D 2018 Zero-static power radio-frequency switches based on MoS2 atomristors *Nat. Commun.* **9** 2524
[24] Chen B, Gao B, Sheng S W, Liu L F, Liu X Y, Chen Y S, Wang Y, Han R Q, Yu B and Kang J F 2011 A novel operation scheme for oxide-based resistive-switching memory devices to achieve controlled switching behaviors *IEEE Electron Device Lett.* **32** 282–4
[25] Lian W *et al* 2011 Improved resistive switching uniformity in $\hbox{Cu/HfO}_{2}/\hbox{Pt}$ devices by using current sweeping mode *IEEE Electron Device Lett.* **32** 1053–5
[26] Zhou F, Chang Y-F, Fowler B, Byun K and Lee J C 2015 Stabilization of multiple resistance levels by current-sweep in SiOx-based resistive switching memory *Appl. Phys. Lett.* **106** 063508
[27] Splendiani A, Sun L, Zhang Y, Li T, Kim J, Chim C Y, Galli G and Wang F 2010 Emerging photoluminescence in monolayer MoS2 *Nano Lett.* **10** 1271–5
[28] Li H, Zhang Q, Yap C, Tay B, Edwin T, Olivier A and Baillargeat D 2012 From bulk to monolayer MoS2: evolution of Raman scattering *Adv. Funct. Mater.* **22** 1385–90
[29] Lanza M 2014 A review on resistive switching in high-k dielectrics: a nanoscale point of view using conductive atomic force microscope *Materials (Basel)* **7** 2155–82
[30] Jana D, Roy S, Panja R, Dutta M, Rahaman S Z, Mahapatra R and Maikap S 2015 Conductive-bridging random access memory: challenges and opportunity for 3D architecture *Nanoscale Res. Lett.* **10** 188
[31] Sun W, Gao B, Chi M, Xia Q, Yang J J, Qian H and Wu H 2019 Understanding memristive switching via in situ characterization and device modeling *Nat. Commun.* **10** 3453
[32] Murthy A A, Stanev T K, Dos Reis R, Hao S, Wolverton C, Stern N P and Dravid V P 2020 Direct visualization of electric-field-induced structural dynamics in monolayer transition metal dichalcogenides *ACS Nano* **14** 1569–76
[33] Iyikanat F, Sahin H, Senger R T and Peeters F M 2014 Ag and Au atoms intercalated in bilayer heterostructures of transition metal dichalcogenides and graphene *APL Mater.* **2** 092801